Journal of Molecular Catalysis A: Chemical 344 (2011) 37–46

Contents lists available at ScienceDirect

Journal of Molecular Catalysis A: Chemical

journal homepage: www.elsevier.com/locate/molcata

Decomposition of ethylene on transition metal surfaces M(1 1 1). A comparative DFT study of model reactions for M = Pd, Pt, Rh, Ni

Duygu Basaran[a], Hristiyan A. Aleksandrov[a,b], Zhao-Xu Chen[a,c], Zhi-Jian Zhao[a], Notker Rösch[a,*]

[a] Department Chemie and Catalysis Research Center, Technische Universität München, 85747 Garching, Germany
[b] Faculty of Chemistry, University of Sofia, 1126 Sofia, Bulgaria
[c] Institute of Theoretical and Computational Chemistry, Key Laboratory of Mesoscopic Chemistry of MOE, School of Chemistry and Chemical Engineering, Nanjing University, Nanjing 210093, PR China

ARTICLE INFO

Article history:
Received 3 February 2011
Received in revised form 26 April 2011
Accepted 26 April 2011
Available online 5 May 2011

Keywords:
Ethylene
Vinyl
Acetylene
Ethynyl
C_2 species
Dehydrogenation reactions

ABSTRACT

Using a periodic slab-model density-functional approach we compared the decomposition of ethylene on the M(1 1 1) surfaces of the transition metals M = Pd, Pt, Rh, and Ni. The set of model reactions included four dehydrogenation steps and one final C–C bond breaking: C_2H_4 (ethylene) → C_2H_3 (vinyl) → C_2H_2 (acetylene) → C_2H (ethynyl) → C_2 (carbon dimer) → C + C. The dehydrogenation steps of ethylene and vinyl are more facile than those of acetylene and ethynyl. Dehydrogenation reactions occur easier, both kinetically and thermodynamically, on Ni(1 1 1) and Rh(1 1 1) than on Pd(1 1 1) and Pt(1 1 1). C_2 decomposition is an exothermic process on Pd(1 1 1), Pt(1 1 1), and Rh(1 1 1), whereas the formation of C_2, a precursor of graphene and coke, is kinetically and thermodynamically most plausible on Ni(1 1 1). The calculated results reveal trends of the binding energies (BE) of the species on the four metals in the order $BE(C_2H_4) < BE(C_2H_2) < BE(C_2H_3) < BE(C_2H) < BE(C_2) < BE(C)$. The binding energies of ethylene and vinyl are largest on Pt(1 1 1) while other species with a lower hydrogen content exhibit the largest BE values on the surfaces Rh(1 1 1) and Ni(1 1 1). We also explored the effect of coverage on the binding energies.

1. Introduction

Unsaturated hydrocarbons are important compounds for the chemical and petrochemical industry due to their high reactivity and the possibility of producing a large variety of valuable products. Usually transition metals are used to catalyze the transformations of unsaturated hydrocarbons; therefore the interaction of these molecular species with the solid surfaces has been a subject of great interest in catalysis. Ethylene, being the simplest unsaturated hydrocarbon, has been studied extensively as these results shed light on pertinent processes including those of more complex unsaturated compounds [1].

On transition metal surfaces, ethylene exhibits two adsorption modes. π-bonded ethylene is more easily hydrogenated [2] whereas ethylene in the more stable, di-σ-bonded mode is proposed to take part in dehydrogenation reactions [3–7]. The reactions of ethylene on group VIII metals give rise to a very complex reaction network, including four types of reactions: dehydrogenation, hydrogenation, 1,2-hydrogen shift, and C–C bond scission [8]. Experimentally it is difficult to determine reaction energies and barriers of the individual reaction steps; therefore theoretical studies are often used to clarify the detailed mechanism of ethylene transformations on the various transition metal surfaces, e.g., on Pd(1 1 1) [3,5,6,8–12], Pt(1 1 1) [7,13,14], Rh(1 1 1) [4], and Ni(1 1 1) [15]. In a previous study, we located all intermediates and transition states that may occur during ethylene decomposition on Pd(1 1 1) [8]. We found most species to undergo C–H bond scission rather than C–C bond breaking due to higher barriers for the latter reaction steps. For ethynyl HCC and bare C_2, we calculated the lowest barriers and the lowest reaction energies of C–C bond breaking. Thus these C_2 species with a minor hydrogen content likely are the precursors of C_1 species noted to modify catalyst particles in transformations of unsaturated hydrocarbons.

Experimentally it is found that at room temperature ethylene converts to ethylidyne on various transition metals [16–19]. In our previous studies we considered several pathways of ethylene conversion to ethylidyne on Pd(1 1 1) [6,9] and Pt(1 1 1) [7]. The hydrogenation/dehydrogenation steps on Pt(1 1 1) have barrier heights in the range 19–95 kJ mol^{-1}, while the corresponding energies are slightly larger on Pd(1 1 1), 25–120 kJ mol^{-1}. The rate-limiting activation barriers are lower on Pt(1 1 1), in line with the experimentally observed faster reaction on Pt(1 1 1) [20]. Andersin et al. examined computationally the transformation of ethylene to ethylidyne, as well as the decomposition of ethylene [11] on flat Pd(1 1 1) and stepped Pd(2 1 1) surfaces [5]. In general, their results

* Corresponding author.
E-mail addresses: roesch@theochem.tu-muenchen, roesch@mytum.de (N. Rösch).

1381-1169/$ – see front matter © 2011 Elsevier B.V. All rights reserved.
doi:10.1016/j.molcata.2011.04.019

showed that the barriers of hydrogenation/dehydrogenation steps are similar for both types of surfaces. Li et al. modeled ethylene conversion to ethylidyne on Rh(1 1 1) [4] and determined that it includes the same most plausible pathway as on Pd(1 1 1), but with a different rate limiting step.

Even at Pt(1 1 1) and Pd(1 1 1), which are well-known for the close similarity of their reactive properties, some differences can be found in the reaction steps under study [7]. Thus, ethylene and other C_2H_x species may behave differently on various transition metals. Hence a comprehensive study of those species including more catalytic metals is of interest for comparing such key reactions as dehydrogenation and hydrogenation, as well as C–C bond scission. Modeling various C_2H_x species and H on several mono- and bi-metallic transition metal substrates, Goda et al. [21] found separate linear correlations for 3d, 4d and 5d-metals between binding energies of C_2H_x and d-band center of the substrate. They also reported reaction barriers for ethyl and vinyl dehydrogenation; however these quantities were derived only from the binding energies of the C_2H_x species invoking the concept of bond order conservation. Medlin and Allendorf modeled acetylene and H adsorption on the surfaces studied in this work, the (1 1 1) surfaces of Pd, Pt, Rh, and Ni [22], but they did not report calculated reaction barriers. On Pd, Pt, and Rh they calculated acetylene to adsorb above three-fold hollow sites, but on Ni(1 1 1) the adsorption complex of acetylene above two neighboring hollow sites was calculated energetically most stable.

The present study aimed at modeling in a systematic fashion the behavior of C_2H_x species (ethylene, vinyl, acetylene, ethynyl, carbon dimer) on the four M(1 1 1) surfaces, M = Pd, Pt, Rh, and Ni. The complete reaction network of ethylene decomposition comprises a rather large number of reaction steps [8]; hence, we restricted this comparative study to a model decomposition of ethylene, namely four consecutive dehydrogenation steps, followed by C–C bond scission: $CH_2CH_2 \rightarrow CH_2CH \rightarrow CHCH \rightarrow CCH \rightarrow C_2 \rightarrow C + C$. The last reaction step is important to exploring on which metals C_2 formation is favorable, as such small carbon species can be considered as precursors of the formation of graphene [23]. Previous studies [4–7,14] showed H-shift reactions to feature significantly higher barriers than the other types of reactions; therefore we did not include such shift reactions in the present work. However, we did explore coverage effects on the binding energies.

2. Models and computational details

The calculations were carried out with the plane-wave based Vienna *ab initio* simulation package (VASP) using a method based on density functional theory (DFT) [24,25]. The interaction between ions and electrons was described by the projector augmented wave (PAW) method [26,27]. The exchange-correlation functional was employed in the gradient-corrected form (generalized gradient approximation – GGA) suggested by Perdew and Wang (PW91) [28]. The Brillouin zone was sampled by a Monkhorst–Pack mesh [29] of $5 \times 5 \times 1$ k points, in combination with first-order Methfessel–Paxton smearing (width of 0.15 eV) [30] to accelerate the convergence; results were extrapolated to no smearing. The energy cut-off was chosen at 400 eV. Spin-polarized calculations were carried out for models of Ni(1 1 1) and hydrocarbon radicals in the gas phase.

The ideal M(1 1 1) surfaces of M = Pd, Pt, Rh, and Ni were modeled as four-layer slabs, repeated in a supercell geometry with a vacuum spacing of at least 1 nm between them. The adsorbates were bound to one side of the slab models, and were allowed to relax during geometry optimizations together with the two adjacent ("upper") layers of the substrate. The two "bottom" layers of the slabs were kept fixed at the theoretical bulk-terminated geometries: Pd: 280 pm, Pt: 282 pm, Rh: 272 pm, and Ni: 248 pm. In the geometry optimizations, all atomic coordinates were relaxed until the force acting on each atom dropped below 2×10^{-4} eV/pm. Coverage effects were explored using three types of unit cells, $(\sqrt{3} \times \sqrt{3})R30^\circ$, (2×2), and (3×3), corresponding to surface coverages 1/3, 1/4, and 1/9, respectively. The transition states were located only at the lowest coverage, 1/9. We estimate the uncertainty of the resulting BE values to about 15 kJ mol^{-1}, in view of the largest difference between the slab model results with four and five layers for the di-σ complex of ethylene on Pt(1 1 1); regarding the k-point grid and the vacuum spacing, the uncertainty is about 5 kJ mol^{-1}.

The reported binding energies (BE) of the adsorbates were calculated as $BE = E_{ad} + E_{sub} - E_{ad/sub}$, where E_{ad} is the total energy of the adsorbate in the gas phase (ground state), E_{sub} is the total energy of the clean substrate, and $E_{ad/sub}$ is the total energy of the substrate, together with the adsorbate in the optimized geometry. With the above definition, positive values of BE imply a favorable interaction, i.e., a release of energy during a reaction.

Transition states (TSs) were determined by applying the dimer method [31] or the nudged elastic band (NEB) method [32,33]. In the latter case we used eight images of the system to form a discrete approximation of the path between fixed end points. In all cases, the pathways identified represent routes connecting the most stable initial and final states. The TS structures obtained in this way were refined until the forces on atomic centers were at most 2×10^{-4} eV/pm. For each transition state structure we checked with a normal mode analysis for only a single imaginary frequency which corresponds to the breaking and formation of the bond of interest. Zero point energy (ZPE) corrections were not applied as our calculations on Pd(1 1 1) had shown that this will reduce barriers only by relatively small amounts, ~10–15 kJ mol^{-1} for C–H breaking and 5–8 kJ mol^{-1} for C–C scission [8]. Li et al. found that the barriers of C–H breaking on Rh(1 1 1) were reduced by at most 18 kJ mol^{-1} [4]. Nave et al. reported ZPE corrections by 10–14 kJ mol^{-1} for C–H scission of methanol on Ni(1 1 1) and Pt(1 1 1) [34].

3. Results: reaction energetics

To be concise, we focus here on the energetics of the four dehydrogenation and one C–C bond breaking reactions involved in our model ethylene decomposition over four transition metal (1 1 1) surfaces; see Tables 1 and 2, as well as Fig. 1 and Figs. S1–S5 of Supplementary Data (SD). Descriptions of the studied adsorption complexes of C and C_2H_x species (x = 0–4) on M(1 1 1) at three different coverages, 1/3, 1/4, and 1/9, are provided as SD.

Table 2 presents information on the transition state structures located as well as the reaction energies and the corresponding reaction barriers at the lowest coverage studied (1/9). Fig. 1 shows the structures of the initial states, the transition states, and the final states of all reaction steps considered for the example of Pd(1 1 1). On all surfaces we considered the same type of adsorption sites, separately for the initial and the final state structures; hence, H was coadsorbed at the same type of sites in the final states. Fig. S1 of SD illustrates all coordination modes of the various adsorbates examined while Figs. S2–S5 of SD compare the same information as Fig. 1 for all surfaces M(1 1 1) studied, M = Pd, Pt, Rh, and Ni together with the lengths of pertinent bonds.

3.1. Ethylene dehydrogenation, TS1

The C–H bond at the transition state of ethylene dehydrogenation is notably elongated on all metal surfaces studied: from 110 pm (Table 1) in di-σ-bonded ethylene to a distance between 155 pm and 174 pm (Table 2). The dissociating H in the transition state is

Table 1
Optimized geometries[a] (pm) and energy characteristics (kJ mol^{-1}) of C_nH_x (n = 1–2, x = 0–4) at 1/9 coverage on M(1 1 1), M = Pd, Pt, Rh, and Ni.

		C–C	C–H	M–C[b]	BE[c]	E_{int}[d]	ΔE(M)[e]	$\Delta E(C_2H_x)$[f]
C_2H_4	Pd	145	110	212; 212	94	190	8	87
	Pt	149	110	212; 212	109	256	15	132
	Rh	147	110	214; 214	86	212	14	112
	Ni	145	110	201; 201	63	166	15	88
C_2H_3	Pd	145	110	203, 203; 208	281	456	7	168
	Pt	147	110	207, 207; 209	309	517	16	192
	Rh	146	110	206, 206; 210	293	488	15	181
	Ni	145	110	189, 200, 201; 206	280	365	11	74
C_2H_2	Pd	137	109	200,218; 200,218	202	430	8	220
	Pt	139	109	201, 221; 201, 221	220	496	22	254
	Rh	139	110	202, 217; 202, 217	240	503	16	247
	Ni	140	110	195, 201, 201; 195, 201, 201	251	543	13	280
C_2H	Pd	137	109	197, 201, 201; 212, 229, 229	474	556	32	50
	Pt	141	109	198, 202, 212; 211, 211, 269	454	603	76	73
	Rh	139	109	196, 205, 205; 221, 221, 223	522	612	26	64
	Ni	137	109	181, 191, 191; 200, 208, 208	527	598	20	51
C_2	Pd	135		199, 211, 211; 198, 213, 213	635	741	39	67
	Pt	136		198, 213, 213; 198, 214, 214	619	774	83	71
	Rh	138		200, 210, 210; 200, 213, 213	698	811	37	76
	Ni	134		185, 198, 198; 184, 199, 199	708	801	30	63
C(fcc)	Pd			188, 188, 188	684	704	20	
	Pt			191, 191, 191	695	732	37	
	Rh			190, 190, 190	690	718	28	
	Ni			176, 176, 176	668	683	15	
C(hcp)	Pd			188, 188, 188	684	696	12	
	Pt			192, 192, 192	678	700	22	
	Rh			191, 191, 191	709	727	18	
	Ni			176, 176, 176	674	688	14	

[a] A – B, distance between atoms A and B.
[b] The C atom that binds to more surface atoms is listed first.
[c] Binding energy of C_nH_x.
[d] Interaction energy of C_2H_x.
[e] Deformation energy of the metal surface.
[f] Deformation energy of the adsorbate. For the definition of these energies, see Section 4.1.

Table 2
Optimized geometries[a] (pm) and energy characteristics (kJ mol^{-1}) of transition states[b] during the model ethylene decomposition on M(1 1 1), M = Pd, Pt, Rh, and Ni, at 1/9 coverage.

		E_r[b]	E'_r[b]	E_a[c]	C–C	C–H[d]	M–C[e]	M–H[d]
TS1[f]	Pd	25	9	99	145	174	207, 210; 208	159
	Pt	25	13	81	148	155	209, 220; 209	162
	Rh	−1	1	45	147	164	210, 211; 210	161
	Ni	−7	−15	47	142	173	190, 202, 207; 203	149
TS2[f]	Pd	−11	−24	76	138	160	201, 215; 205, 231	163
	Pt	14	3	85	140	148	200, 221; 212, 221	162
	Rh	−37	−38	21	140	152	201,216; 208, 218	162
	Ni	−58	−68	50	143	143	193, 218, 220; 190, 192, 245	153
TS3[f]	Pd	31	25	119	137	176	197, 201, 207; 210, 217, 258	159
	Pt	83	79	143	141	159	197, 211, 214; 210, 211, 275	166
	Rh	27	28	96	139	162	196, 202, 203; 222, 224, 225	165
	Ni	29	26	111	136	177	179, 189, 189; 200, 211, 211	149
TS4[f]	Pd	72	61	154	134	181	200, 214, 214; 197, 212, 212	158
	Pt	85	73	143	136	159	198, 215, 215; 201, 214, 214	165
	Rh	60	58	131	137	164	197, 210, 210; 202, 212, 212	164
	Ni	57	46	131	134	176	181, 195, 196; 186, 199, 200	149
TS5[g]	Pd	1	−63	121	194		190, 199, 204; 190, 199, 204	
	Pt	−46	−101	135	188		192, 197, 237; 193, 204, 205	
	Rh	−16	−50	113	224		185, 192, 205; 182, 194, 237	
	Ni	71	29	142	199		177, 183, 185; 177, 183, 185	

[a] A – B, distance between atoms A and B in the transition state.
[b] Reaction energy E_r for the case of co-adsorbed product species, while E'_r values correspond to the product fragments at infinite separation.
[c] Activation energy.
[d] Distance characterizing a bond that forms or breaks during the reaction.
[e] The C atom that binds to more surface atoms is listed first.
[f] Transition state of a dehydrogenation reaction.
[g] Transition state of C–C scission.

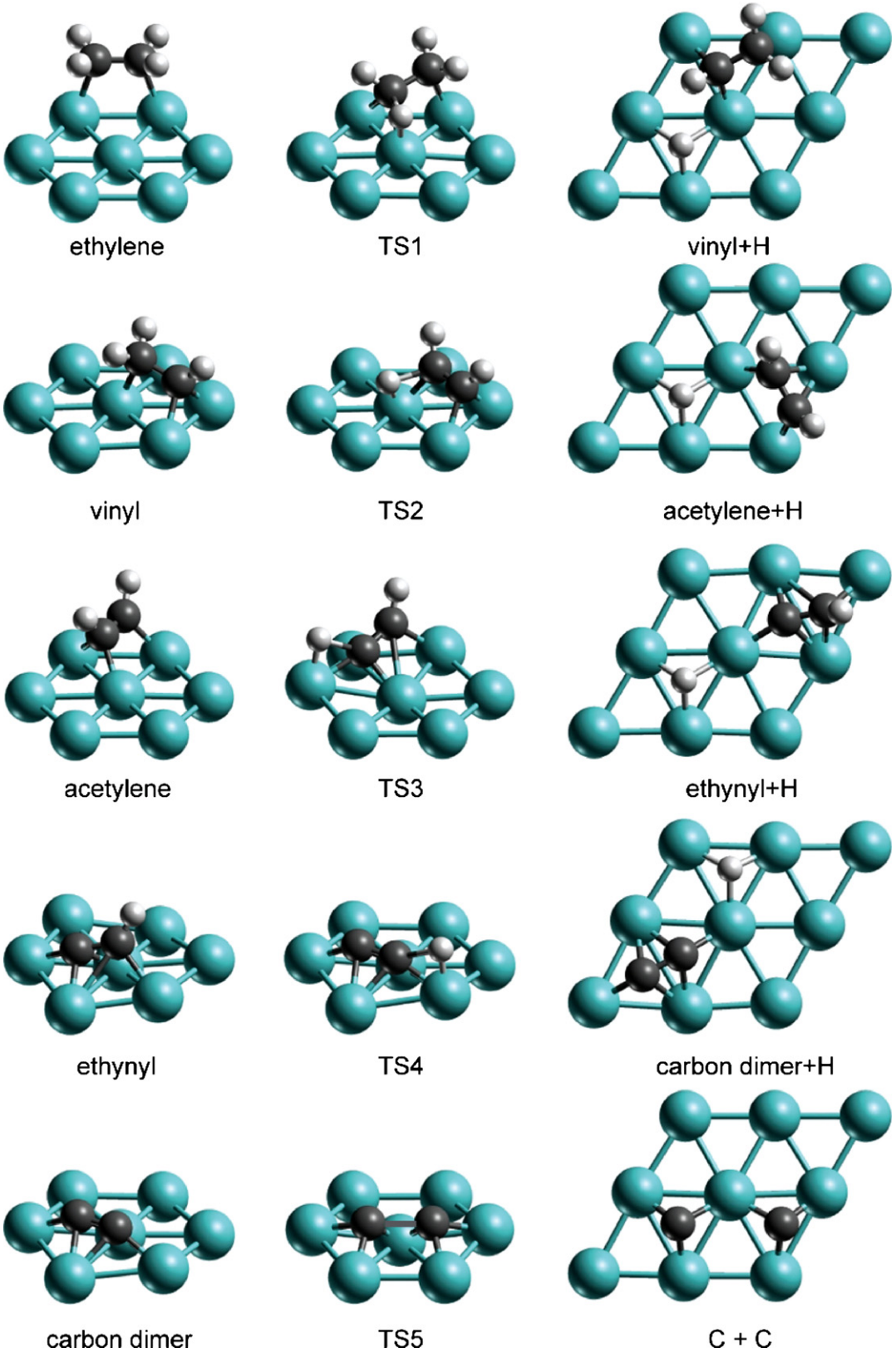

Fig. 1. Structures of initial, transition, and final states at 1/9 coverage of the model decomposition of ethylene which includes five reaction steps: $C_2H_4 \rightarrow TS1 \rightarrow C_2H_3 + H$, $C_2H_3 \rightarrow TS2 \rightarrow C_2H_2 + H$, $C_2H_2 \rightarrow TS3 \rightarrow C_2H + H$, $C_2H \rightarrow TS4 \rightarrow C_2 + H$, and $C_2 \rightarrow TS5 \rightarrow C + C$ on Pd(1 1 1). The corresponding structures of all metals studied are available as Supplementary Data.

bound on top of a nearby metal atom, M–H = 149–162 pm. On the (1 1 1) surfaces of Pd, Pt and Rh the C atom, from which the H atom has been subtracted, moves to a bridge position and forms a second M–C bond. On Ni(1 1 1), however, it moves to the threefold site, forming two additional Ni–C bonds (Fig. S5 of SD). On all four transition metal surfaces, the transition state has a "late" character as the structure is similar to the product complex where vinyl is co-adsorbed with H.

The dehydrogenation of ethylene to vinyl is slightly exothermic on Ni(1 1 1), energetically neutral on Rh(1 1 1), but slightly endothermic on Pd(1 1 1) and Pt(1 1 1) (Table 2). The activation barriers on Rh and Ni surfaces are very similar, 45 kJ mol^{-1} and 47 kJ mol^{-1}, respectively; these values are significantly smaller, at least by 34 kJ mol^{-1}, than the barriers on Pt, 81 kJ mol^{-1}, and Pd, 99 kJ mol^{-1}.

This reaction step was addressed also in a variety of other computational studies, on Pd(1 1 1) [3,5,6,8,9,11], Pt(1 1 1) [7,14], Rh(1 1 1) [4], and Ni(1 1 1) [15]. The present results for Pd(1 1 1) and Pt(1 1 1) are similar to our previous results [6–9] when we used five-layer slab models of the metals. The corresponding energy differences are small, 1 kJ mol^{-1} for Pd(1 1 1) and 6 kJ mol^{-1} for Pt(1 1 1). Elsewhere we already discussed in detail [6] differences to the previous results of Pallassana et al. [3]. On the other hand, Li et al. [4] determined the reaction energy of this reaction step on Rh(1 1 1), 2 kJ mol^{-1}, and the corresponding barrier, 50 kJ mol^{-1}, in very good agreement with our present results, 1 kJ mol^{-1} and 45 kJ mol^{-1}, respectively. Our results for Pt(1 1 1) also agree well with those of Chen and Vlachos [14] who found that this reaction step is slightly endothermic, 2 kJ mol^{-1} with a barrier of 81 kJ mol^{-1}. Vang et al. [15] calculated ethylene dehydrogenation on Ni(1 1 1) to be endothermic by 20 kJ mol^{-1}, with a barrier of ~60 kJ mol^{-1}. The notable differences to our results for Ni(1 1 1) likely are due to the simplified model used in those previous calculations [35].

3.2. Vinyl dehydrogenation, TS2

During vinyl dehydrogenation to acetylene, one of the C–H bonds of the CH_2 group elongates from 110 pm in the initial state (Table 1) by similar amounts as in the case of ethylene (see above), to 143–160 pm in the TS2 structures. The dissociating H atom starts to interact with the surface metal atom to which the CH_2 group of vinyl was bound (Fig. 1 and Figs. S2–S5 of SD for details). In TS2, the M-H distances, 153–163 pm, are similar to the corresponding distances of TS1 (Table 2). On the (1 1 1) surfaces of Pd, Pt, and Rh, the C atom of the original CH_2 group moves to a bridge site where it interacts with a second metal atom, the one already bonded to the CH group of the vinyl species. Hence in the final state, acetylene is adsorbed above a hollow site in a $\eta^2\eta^2$ fashion (Fig. S1 of SD). Only on Ni(1 1 1), the C atoms move to neighboring hollow positions and acetylene forms an adsorption complex of $\eta^3\eta^3$ type (Figs. S1 and S5 of SD).

On all surfaces studied, the dehydrogenation of vinyl to acetylene was determined energetically more favorable than the corresponding dehydrogenation of ethylene. This step is still endothermic on Pt(1 1 1), by 14 kJ mol^{-1}, but exothermic on Pd, Rh, and Ni (1 1 1) (Table 2). The highest barrier, 85 kJ mol^{-1}, of vinyl dehydrogenation was obtained for Pt(1 1 1) while on Rh(1 1 1) the barrier is significantly lower, only 21 kJ mol^{-1} (Table 2). On Pd(1 1 1) the barrier, 76 kJ mol^{-1}, is quite close to that on Pt(1 1 1). The barrier calculated for Ni(1 1 1), 50 kJ mol^{-1}, agrees well with the value of a previous theoretical study [15]. On Pt(1 1 1), Chen and Vlachos [14] calculated a barrier, 99 kJ mol^{-1}, that is notably higher than our value, 85 kJ mol^{-1}. The reaction energy also differs somewhat; it is endothermic by 2 kJ mol^{-1}, compared to our result, endothermic by 14 kJ mol^{-1}. This discrepancy likely is caused by different choices of unit cells, (2 × 2) in Ref. [14] and (3 × 3) in the present work, as suggested by the remark [14] that barriers are lowered by ~10 kJ mol^{-1} when one switches from a (2 × 2) to a (3 × 3) surface unit cell.

3.3. Acetylene dehydrogenation, TS3

The structures of TS3, during the dehydrogenation of acetylene to ethynyl, were calculated similar on all four metals. In the structures on the (1 1 1) surfaces of Pd, Pt, and Rh, the CCH moiety of the TS3 is oriented in the same fashion as ethynyl in the structure of the corresponding final state; hence these transition states have a "late" character. The CH moiety and the second C center move to two neighboring threefold sites; the C atom from which H is subtracted forms an additional bond with a surface atom. Initial and final state complexes are similarly adsorbed on Ni(1 1 1), in $\eta^3\eta^3$ fashion, the only notable difference being the leaving H atom. In the TS3 structures, similar to the previous dehydrogenation steps, the M–H distances are 149–166 pm and the C–H distances are elongated to 159–177 pm (Table 2); on all surfaces, the H atom moves to a top site in the transition state.

Experiments showed that acetylene, adsorbed on (1 1 1) surfaces of late transition metals, converts to vinylidene, ethynyl, methylidyne, ethylidyne, and surface carbon at low temperatures [36–39]. Acetylene was reported to dehydrogenate to ethynyl on Rh(1 1 1), Pd(1 1 1), and Ni(1 1 1) [36], but to convert preferentially to vinylidene on Pt(1 1 1) [36,38]. In agreement with these experimental findings, we calculated the dehydrogenation of acetylene to ethynyl on Pt(1 1 1) to be strongly endothermic, by 83 kJ mol^{-1}, with a reaction barrier of 143 kJ mol^{-1} (Table 2). In contrast, on the (1 1 1) surfaces of Pd, Rh, and Ni, the reaction energies are notably less endothermic, 31 kJ mol^{-1}, 27 kJ mol^{-1}, and 29 kJ mol^{-1}, respectively, while the corresponding activation barriers were determined significantly lower than for Pt(1 1 1), at 119 kJ mol^{-1}, 96 kJ mol^{-1}, and 111 kJ mol^{-1} (Table 2). Another experiment [40] found that acetylene converts to vinylidene on Pd(1 1 1); however, our recent theoretical study [8] showed that a such process likely proceeds in two steps: acetylene first is dehydrogenated to ethynyl which, in turn, is then hydrogenated to vinylidene.

3.4. Ethynyl dehydrogenation, TS4

Also the dehydrogenation of ethynyl to a carbon dimer starts with the C–H bond elongating, from 109 pm (Table 1) to 159–181 pm in TS4, as the H center moves over a top position and, at M–H distances of 149–165 pm, starts to interact with a metal center (Table 2).

On all metal surfaces examined, the last dehydrogenation step to the carbon dimer is the most endothermic one among the four consecutive C–H bond breaking steps of ethylene. For Pt(1 1 1), the reaction energy is close to the value of acetylene dehydrogenation, but on the (1 1 1) surfaces of Pd, Rh, and Ni, this energy is more than 28 kJ mol^{-1} higher (Table 2). The highest activation barrier, 154 kJ mol^{-1}, was calculated for Pd(1 1 1); this also is the highest barrier in the whole chain of reactions. On Pt(1 1 1), the barrier is only 11 kJ mol^{-1} lower, 143 kJ mol^{-1}, and on both Rh(1 1 1) and Ni(1 1 1), it is 131 kJ mol^{-1} (Table 2).

3.5. Carbon dimer dissociation, TS5

The last step of our model ethylene decomposition is the dissociation of the carbon dimer species, followed by the migration of one of the C atoms to a neighboring fcc-threefold site. On Pt(1 1 1), Ni(1 1 1), and Pd(1 1 1), both carbon atoms move close to bridge positions. As the metal surface is distorted, each C atom continues to interact with three metal atoms, with the exception of Pt(1 1 1) where one of the carbon atoms interacts with two metal atoms

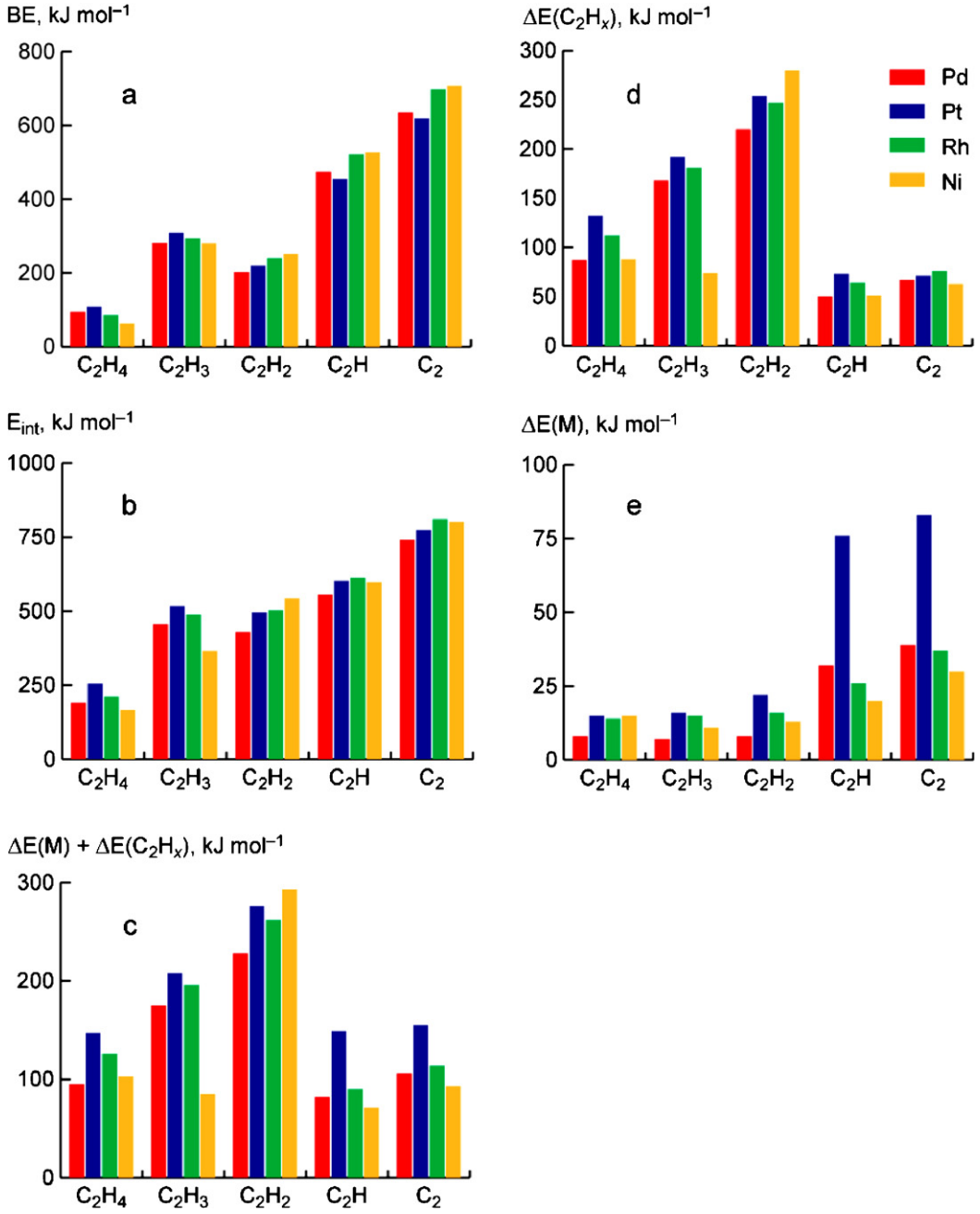

Fig. 2. Various characteristic energies (kJ mol^{-1}) of the adsorbates on four metal surfaces: (a) binding energies: BE, (b) metal–adsorbate interaction: E_{int}, (c) total deformation energies of the surface and the hydrocarbon species due to adsorption: $\Delta E(M) + \Delta E(C_2H_x)$, (d) deformation energies of the hydrocarbon species: $\Delta E(C_2H_x)$, and (e) deformation energies of the surfaces: $\Delta E(M)$.

only. On Pt(1 1 1), Ni(1 1 1), and Pd(1 1 1), the C–C distance elongates from 134–136 pm (Table 1) in the initial state to 188–199 pm in TS5 (Table 2). In contrast, on Rh(1 1 1), one of the C atoms remains at the initial hollow position, while the other one moves to a bridge site in the transition state, with C–C = 224 pm; in the final state, this C center arrives at another fcc-hollow site.

C–C bond breaking is exothermic on Pt(1 1 1), −46 kJ mol^{-1}, and Rh(1 1 1), −16 kJ mol^{-1}, energetically neutral on Pd(1 1 1), and strongly endothermic on Ni(1 1 1), 71 kJ mol^{-1} (Table 2). The barriers of C–C bond breaking are above 110 kJ mol^{-1} on all metal surfaces studied. Although C–C scission is exothermic on Pt(1 1 1), the corresponding activation barrier, 135 kJ mol^{-1}, is among the highest in the model reaction scheme of this metal. Andersin et al. [11] calculated the barrier of this step on Pd(1 1 1) for 1/6 coverage at 138 kJ mol^{-1}, i.e., by ∼20 kJ mol^{-1} higher than our results, 121 kJ mol^{-1} for 1/9 coverage; in turn, the endothermicity obtained in that study was 28 kJ mol^{-1}, in contrast to our result, 1 kJ mol^{-1}.

4. Discussion

4.1. Binding energies

Fig. 2a compares the binding energy of the species C_2H_x (x = 0–4) as calculated for the four metal surfaces M(1 1 1) at 1/9 coverage. The BE values of ethylene decrease in the order Pt > Pd > Rh > Ni (Fig. 2a and Table 1). The binding energy of C_2H_3 is again largest on Pt(1 1 1) and smallest on Ni(1 1 1), whereas the trend is opposite

for the species with less hydrogen content (acetylene, ethynyl, C_2): Ni > Rh > Pd > Pt. On each metal, the binding energies of the various species follow the same trend: $C_2H_4 < C_2H_2 < C_2H_3 < C_2H < C_2 < C$; for C, see Table 1. Except for C_2H_2 and C_2H_3, this trend is consistent with the concept of bond order conservation: the fewer H ligands at the carbon centers, the stronger the interaction with the substrate.

To analyze the binding energies in more detail, we decomposed these quantities into various contributions according to $BE = E_{int} - \Delta E(M) - \Delta E(C_2H_x)$. Here E_{int} is the (full) metal–adsorbate interaction; $\Delta E(M)$ and $\Delta E(C_2H_x)$ are the deformation energies of the metal surface and the adsorbate, respectively, i.e., those energy changes that are required to bring a system from its equilibrium structure to the structure displayed in the adsorption complex. The resulting E_{int} values (Fig. 2b and Table 1) resemble those of the corresponding BE values. In general the trends of the binding energies can be rationalized using the (full) metal–adsorbate interaction. Inspection of the binding energy or the full interaction energy and the sum of deformation energies clearly reveals that the irregular energetic behavior of C_2H_2 (with respect to C_2H_3) is due to the larger deformation energy accompanying the adsorption of acetylene (Fig. 2c).

Further analysis shows that the larger sum of deformation energies of C_2H_2 is due to the deformation of the adsorbate, not of the substrate (Fig. 2d and e). In fact, except for C_2H and C_2 on Pt where the substrate deforms in a major way, adsorbate deformation always contributes the most to the total deformation of the adsorption system. As a trend deformation energies of the adsorbates increase significantly from 87–132 kJ mol^{-1} to 220–280 kJ mol^{-1} in the order ethylene < vinyl < acetylene (Fig. 2d and Table 1). Subsequently, for the species with less H content, they decrease dramatically, to 50–76 kJ mol^{-1}, for ethynyl and C_2 (Fig. 2d and Table 1). In contrast, for ethylene, vinyl, and acetylene, the deformation energies of the metal surfaces are rather small, typically below 20 kJ mol^{-1}, on each metal, but they increase up to 83 kJ mol^{-1}, for the species with low H content, ethynyl and C_2 (Fig. 2e and Table 1). This increase is remarkably higher on Pt(1 1 1) (and to some extent also on Pd(1 1 1)) than on Rh(1 1 1) and Ni(1 1 1). As the deformation energies of the adsorbates in most cases are significantly larger than those of the metal surfaces, in general the total deformation energies (Fig. 2c) follow the trend of $\Delta E(C_2H_x)$ (Fig. 2d).

We also explored how much on average metal atoms in the top layer are displaced upon adsorption of the hydrocarbon species. This average displacement increases as the H content of the adsorbate decreases, correlating with an exponentially growing $\Delta E(M)$ (Fig. 3).

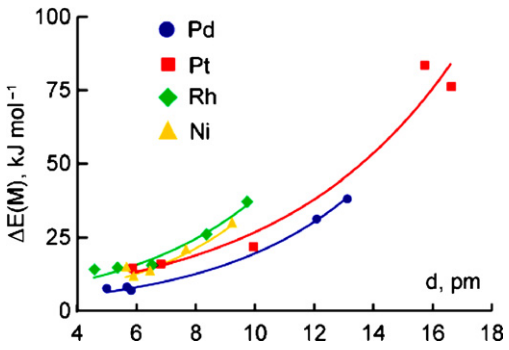

Fig. 3. Exponential correlation of deformation energies ΔE (kJ mol^{-1}) of the surfaces as function of the average displacements, d (pm), of the metal atoms in the top layer: Pd: $(2.35 \pm 0.30) \times \exp[(0.21 \pm 0.01)d]$, $r = 1.00$; Pt: $(4.93 \pm 2.52) \times \exp[(0.17 \pm 0.03)d]$, $r = 0.98$; Rh: $(4.35 \pm 0.93) \times \exp[(0.22 \pm 0.02)d]$, $r = 0.98$; Ni: $(2.87 \pm 0.77) \times \exp[(0.25 \pm 0.03)d]$, $r = 0.97$.

4.2. Barriers and reaction energies

Table 2 lists the geometric and energetic results for the five reaction steps on the four metal surfaces. Apparently, the five reactions can be divided into two groups according to the magnitude of the barrier: dehydrogenation of C_2H_x ($x = 3, 4$) on the one hand, and dehydrogenation or dissociation of C_2H_x ($x = 0$–2) on the other. Typically, on all metals the barriers of the dehydrogenation of C_2H_x ($x = 3, 4$) are more than 50 kJ mol^{-1} lower than the barriers of the second group ($x = 0$–2). The barriers of the second dehydrogenation step, vinyl dehydrogenation, tend to be the lowest, 21–85 kJ mol^{-1}, while the final dehydrogenation barriers, those of ethynyl, are the highest, 131–154 kJ mol^{-1} (Table 2).

The reaction energies show similar trends. The reaction energies of dehydrogenation of ethylene (to vinyl) and of vinyl (to acetylene) are 30 kJ mol^{-1} more exothermic than the reaction energies of the subsequent two dehydrogenation steps, of acetylene (to ethynyl) and ethynyl (to the carbon dimer). Dehydrogenation of vinyl is the most exothermic step, −58 kJ mol^{-1} to 14 kJ mol^{-1}. The most endothermic dehydrogenation step is that of ethynyl, 57–85 kJ mol^{-1}. C_2 species can be regarded as a precursor of forming graphene or coke on the metal surfaces; in this context, the backward reaction, namely the formation of C_2 from two carbon atoms, is of interest. The barriers are high on Pd (120 kJ mol^{-1}), Rh (129 kJ mol^{-1}), and Pt (181 kJ mol^{-1}) while the barrier on Ni(1 1 1) is significantly lower, 71 kJ mol^{-1}, and the reaction is exothermic, by −71 kJ mol^{-1}, thus facilitating C–C bond formation. The easy formation of coke on Ni surfaces, implied by these results, agrees with experimental [41,42] and previous theoretical findings [42,43].

Our calculated energetics also suggested that the four metal surfaces can be divided into two groups. On Rh(1 1 1) and Ni(1 1 1), dehydrogenation reaction steps have lower barriers and are more exothermic than the corresponding processes on Pt(1 1 1) and Pd(1 1 1) (Table 2). The most active metal of the set treated is Rh on which dehydrogenation barriers are even lower than on Ni (by up to 29 kJ mol^{-1}) although on the latter surface the reaction energies are usually more exothermic (by up to 21 kJ mol^{-1}). The endothermicity of C_2 dissociation on these two metals is exactly opposite: this reaction is calculated to be notably exothermic on Rh(1 1 1), −16 kJ mol^{-1}, whereas it is endothermic on Ni(1 1 1), by 71 kJ mol^{-1}. The Pt(1 1 1) surface is the only one among those studied where an energy release (of 46 kJ mol^{-1}) is calculated for C_2 dissociation, whereas the four dehydrogenation steps are endothermic.

To rationalize the energetic trends of the various dehydrogenation reactions on the four metal surfaces, we analyze the surface reactions by a thermodynamic circle, the other steps of which are: (i) desorption of the reactant from the surface, (ii) dehydrogenation in the gas phase, and (iii) adsorption of the products back onto the surface. Hence the reaction energies of the dehydrogenation steps can be divided into three components, assuming infinitely separated product fragments: (i) the difference between the binding energies of reactant and product species, $\Delta BE(C_2H_x \rightarrow C_2H_{x-1}) = BE(C_2H_{x-1}) - BE(C_2H_x)$, (ii) the reaction energy $\Delta E(C_2H_x \rightarrow C_2H_{x-1})$ of the dehydrogenation in the gas phase, and (iii) BE(H). The successive dehydrogenation steps of ethylene in the gas phase are strongly endothermic: 479, 180, 580, and 505 kJ mol^{-1}, respectively (not shown in the tables). The energy changes of three of these steps are similarly large, 479–580 kJ mol^{-1}, whereas the second step, the dehydrogenation of vinyl to acetylene, requires much less energy, 180 kJ mol^{-1}. This notable difference can be rationalized by the fact that in this reaction step a stable species in gas phase, acetylene, is formed, whereas in all other cases the product C_nH_x species are not sta-

ble in the gas phase. On the surfaces these strongly endothermic reaction energies are somewhat compensated by the fact that the binding energies of the products are larger than those of the reactants. The values of $\Delta BE(C_2H_x \rightarrow C_2H_{x-1})$ of the various reactants (for $x = 4$–1) range from 187 kJ mol^{-1} to 217 kJ mol^{-1} for the reactant ethylene, from −89 to −29 kJ mol^{-1} for vinyl, from 234 kJ mol^{-1} to 282 kJ mol^{-1} for acetylene, from 161 kJ mol^{-1} to 181 kJ mol^{-1} for ethynyl. The second step $C_2H_3 \rightarrow C_2H_2$ again forms an exception as $BE(C_2H_3)$ is larger than $BE(C_2H_2)$, due to the same fact that the product is stable in gas phase.

Next we discuss trends of reaction energies on the various metals. At 1/9 coverage the BE(H) values at the hollow sites of M(1 1 1), M = Pd, Pt, Rh, and Ni, agree within 16 kJ mol^{-1}: 267, 283, 271, and 277 kJ mol^{-1}, respectively (not shown in the tables). This small difference renders some of the reaction steps slightly more exothermic on Pd(1 1 1) than on Pt(1 1 1), but it cannot account for the different behavior on different metal surfaces; see also Section 4.4 regarding the lack of a linear correlation between barriers and values of BE(H). Therefore, the values of $\Delta BE(C_2H_x \rightarrow C_2H_{x-1})$ have to be invoked to rationalize the different behavior on the four metals. For example, $\Delta BE(C_2H_3 \rightarrow C_2H_2)$ is −89 kJ mol^{-1} on Pt and −79 kJ mol^{-1} on Pd; these values are lower than those on Rh, −53 kJ mol^{-1}, and −29 kJ mol^{-1} on Ni. Correspondingly, the barriers of TS2 ($C_2H_3 \rightarrow C_2H_2$) on Pt and Pd, above 75 kJ mol^{-1}, are notably higher than those on Rh and Ni, up to 50 kJ mol^{-1} (Table 2).

To discuss the trend of the corresponding reaction barriers, we invoke the frequent finding that lower barriers tend to be associated with less endothermic or more exothermic reactions (see the discussion of the Brønsted–Evans–Polanyi relationship in Section 4.4). The lowest barrier, that of TS2 ($C_2H_3 \rightarrow C_2H_2$), can be rationalized by the smallest endothermicity in the gas phase, 180 kJ mol^{-1}. By the same argument, the lower barrier of TS1 ($C_2H_4 \rightarrow C_2H_3$) can be rationalized by the fact that the product C_2H_3 adsorbs more strongly than the reactant C_2H_4 (Fig. 2a). Although the reaction energy for $C_2H_2 \rightarrow C_2H$ is the most endothermic, 580 kJ mol^{-1}, the large difference of binding energies in favor of the product renders the barrier of this step, TS3, comparable to that of TS4.

A similar thermodynamic circle can be considered for the decomposition of C_2: (i) desorption of the C_2 species from the surface, (ii) decomposition of C_2 in the gas phase, and (iii) adsorption of the C atoms back onto the surface. The corresponding reaction energy can be partitioned into only two components, assuming infinitely separated product fragments: (i) the difference between the binding energies of C_2 and two carbon atoms, $\Delta BE(C_2 \rightarrow C + C) = 2 \times BE(C) - BE(C_2)$, and (ii) the reaction energy $\Delta E(C_2 \rightarrow C + C)$ of C_2 decomposition in the gas phase. The latter contribution, 670 kJ mol^{-1}, is again strongly endothermic; it is compensated by the larger binding energies of the products compared that of the reactant. The exothermicity or endothermicity of the decomposition of C_2 at different metals obviously varies with the value of $\Delta BE(C_2 \rightarrow C + C)$. For instance on Ni(1 1 1), C_2 binds strongest, while the C atoms have the smallest binding energy; hence the reaction is most endothermic on Ni among all metals considered.

4.3. Coverage effect

Next we briefly address how the coverage of the surfaces affects the energetics. We do this by comparing energy changes for two situations: (a) when the products are in the final state of a reaction, and (b) when the reaction products are assumed to be at infinite separation. This effect is particularly significant for the decomposition of C_2 in view of the strong interaction between the two C adsorbates in the final state. Hence all reaction energies become more exothermic, by 34–64 kJ mol^{-1}, when both C species are assumed to be at infinite separation in the final state (Table 2). For comparison, dehydrogenation steps become more exothermic at most by 16 kJ mol^{-1} when the products H and C_2H_x ($x = 0$–3) are taken to be at infinite separation. The coverage effect on the reaction energies of the various metals decreases in the order Pd > Pt > Ni > Rh. In most cases the values of the first three metals are very close while this "coverage" effect is negligible on Rh, especially for the dehydrogenation steps. Barriers for the dehydrogenation reactions decrease with decreasing the coverage. In previous studies of ethylene transformations over Pd(1 1 1) [6,9] and Pt(1 1 1) [7], comparable results had been obtained; there, barriers were calculated higher by 3–30 kJ mol^{-1} when the surface coverage increased from 1/9 to 1/3.

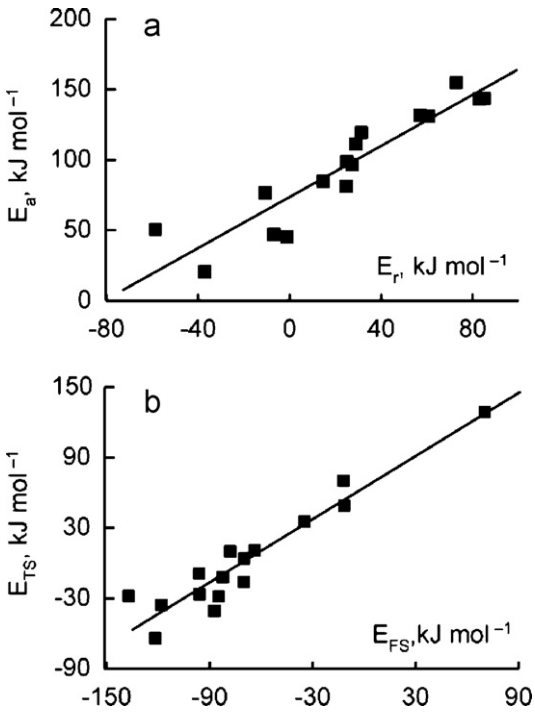

Fig. 4. Linear relationships between (a) reaction energies E_r and activation barriers E_a (kJ mol^{-1}): $E_a = (0.91 \pm 0.10)\, E_r + (73.67 \pm 4.72)$; $r = 0.92$, and (b) "full" energies (see Section 4.4) of the products E_{FS} and the transition states E_{TS}: $E_{TS} = (0.90 \pm 0.08)\, E_{FS} + (64.33 \pm 6.65)$; $r = 0.95$.

4.4. Relationship between reaction energies and activation barriers

The activation energy is a key parameter that controls the rate of each elementary step and as a result determines the reaction path. Recently, the Brønsted–Evans–Polanyi relationship (BEP) [44,45] was shown to apply in heterogeneous catalysis [10,46–49]. The BEP relationship connects the reaction barriers (hence the reaction kinetics) to the thermodynamics (the reaction energies) by stipulating a linear relationship between these two types of quantities, allowing one to estimate barriers from the corresponding reaction energies, provided the reactions are of similar character.

Fig. 4a shows the relationship between activation energies and reaction energies for the dehydrogenation steps over the four metal surfaces; Fig. 4b illustrates the analogous relationship between the "absolute" energies of a transition state, E_{TS}, and the corresponding final state, E_{FS}, measured relative to a common reference, the initial state with ethylene in the gas phase and a clean metal surface. These two plots demonstrate that linear relationships hold very well across these four metals. The close relationship between the energies of the final states and the energies of the transition states suggests that the latter are of a "late" character [50]; this corrobo-

rates our earlier conclusion based on the structures of the transition states (Section 3). Our result, $E_a = (0.91 \pm 0.10)\ E_r + (73.67 \pm 4.72)$ in kJ mol^{-1} ($r = 0.92$), agrees very well with an earlier finding [48] that incorporates dehydrogenation steps of C–H and O–H bonds, $E_a = (0.92 \pm 0.05)\ E_r + (84.26 \pm 4.84)$ ($r = 0.96$).

In Fig. 4a and b, the points above the regression line mainly belong to dehydrogenation reactions on Ni(1 1 1) and Pd(1 1 1), while those below the line are from the reactions on Pt(1 1 1) and Rh(1 1 1). We tried to rationalize this observation with the BE(H) at top positions as H atoms are at such a location in almost all TS structures. These BE(H) values are larger on Pt (262 kJ mol^{-1}) and Rh (239 kJ mol^{-1}) than on Pd (230 kJ mol^{-1}) and Ni (221 kJ mol^{-1}). Further analysis reveals that there are no (linear) correlations between the barriers on the one hand, and BE(H) or BE(C_2H_x) values on the other hand. However, there are (approximate) linear correlations between barriers and ΔBE($C_2H_x \rightarrow C_2H_{x-1}$) values with correlation coefficients r from 0.92 to 0.95, except for the step $C_2H_3 \rightarrow C_2H_2 + H$ for which $r = 0.7$ only due to the result for Ni(1 1 1). This latter exception is related to the fact that the values of BE(C_2H_3) and BE(C_2H_2) are very close; for details, see SD. These findings clearly show that the relative reaction kinetics of C–H bond breaking on transition metal surfaces is controlled by the adsorption interactions of carbon containing species of both reactant and products, while the bonding of H atom with the substrate has much less effect, probably due to the relatively small variations in the values of BE(H).

4.5. Limitations of the models used

Finally, we would like to comment briefly on limitations due to the specific chain of model reactions used in this study. The decomposition of ethylene on transition metal surfaces is quite complex and may include significantly more steps [8] than those five considered in the present work. However, as found in our previous studies, the dehydrogenation of ethylene to vinyl is the crucial, rate-limiting step during the conversion ethylene to ethylidyne on Pd(1 1 1) [6,9] and it is also an important step in that transformation over Pt(1 1 1) [7]. The hydrogenation of acetylene to ethylene also includes reaction steps studied here: $C_2H_2 \rightarrow C_2H_3 \rightarrow C_2H_4$ [51]. In addition, on Pd(1 1 1) and Pt(1 1 1), the precursors of C–C bond breaking were found to be species with few or no hydrogen atoms [8]. With the inclusion of of C–C bond scission in C_2 species in our model chain of reactions, we do not exclude the possibility that this bond is breaking earlier, in a hydrogenated species, as found in a Monte Carlo simulation based on DFT calculations where at high H_2 pressure C_2H_5 was determined to be the most important precursor for the C–C bond cleavage of ethane [52].

Of course, we do not want to imply that the mechanism of ethylene decomposition is determined by exactly those five reaction steps considered here. However, these five steps are among the most important ones in the complex scheme of ethylene transformations on M(1 1 1). They also comprise various representative hydrocarbon species of a different H content. Therefore, trends of C–H and C–C bond breaking identified here should also hold for other transformations of ethylene, e.g., the steps to ethylidyne [4–7,9,11] or those we found to occur on the way to C_1 species, $CH_2C \rightarrow CHC \rightarrow CH + C$ over Pd(1 1 1) [8].

Another limitation of the present study is the restriction to idealized M(1 1 1) surfaces. Catalytic reactions are known to occur preferentially at surface defects, e.g., at step-edge sites [47,53]. For instance, steps and other surface defects have been shown to favor C–C bond breaking on Ni [15]. Also the barrier of the reaction $C_2H_4 \rightarrow CH_2 + CH_2$ was calculated to be higher on Pd(1 1 1), 2.12 eV, than on Pd(2 1 1), 1.69 eV [5,11]. However the barriers of the reaction steps $C_2H \rightarrow C + CH$ and $C_2 \rightarrow C + C$ are quite similar on Pd(1 1 1) and Pd(2 1 1); the second barrier is even lower on Pd(1 1 1). Yet, those studies also calculated barriers of hydrogenation or dehydrogenation steps to be similar on both surfaces.

Finally we would like to point out that coverage effects are idealized when the unit cell is changed, as done in the present model study. Although coverage effects are partially accounted for, such models obviously are, from the viewpoint of catalysis, artificial as they ignore other coexisting species or other possible arrangements of adsorbates.

5. Conclusions

Using periodic slab model density functional calculations at the GGA level, we have carried out a computational study of a model decomposition of ethylene on M(1 1 1) surfaces of M = Pd, Pt, Rh, and Ni, with the five steps: $C_2H_4 \rightarrow C_2H_3 + H$; $C_2H_3 \rightarrow C_2H_2 + H$; $C_2H_2 \rightarrow C_2H + H$; $C_2H \rightarrow C_2 + H$; $C_2 \rightarrow C + C$. We found that the closed-shell molecules ethylene and acetylene, which are stable in gas phase, have the lowest binding energies, 33–109 kJ mol^{-1} (Table S1) and 179–251 kJ mol^{-1} (Table S3), respectively. For the remaining open-shell species, the adsorption energies increase with decreasing H content.

On all metals studied, the binding energies increase in the order: $C_2H_4 < C_2H_2 < C_2H_3 < C_2H < C_2 < C$. The binding energies of C_2H_4 and C_2H_3 were calculated to be highest on Pt(1 1 1), whereas C_2H_2, C_2H, and C_2 feature the largest BE values on Rh(1 1 1) and Ni(1 1 1). The adsorption energies on all metals decrease with increasing coverage, due to larger repulsive lateral interactions. There are only few exceptions (C_2H, C_2) where binding energies at 1/3 coverage, the highest value studied, are higher on some metals than the corresponding values at 1/4 coverage; these exceptions are due to the formation of linear chains, –M–C–C–M–C–C–, at 1/3 coverage; for details, see SD.

Our results in Table 2 show that dehydrogenation reactions will occur easier, both kinetically and thermodynamically, on Ni(1 1 1) and Rh(1 1 1) than on Pd(1 1 1) and Pt(1 1 1). Trends of reaction energies and barriers on the various metals are controlled mainly by the difference between the BE values of reactant C_2H_x and product C_2H_{x-1} species. As Ni is notably cheaper than the other three metals considered, it would be attractive if this metal could replace other metals as a catalyst in various hydrocarbon transformations including dehydrogenation reactions. However, coke formation on Ni presents a serious problem that significantly reduces its potential applicability in catalytic processes. Several recent studies addressed improving the coke resistance of Ni-based catalysts [43,54].

On all metals studied, we determined the first two dehydrogenation steps, ethylene → vinyl → acetylene, to be kinetically and thermodynamically more facile than the dehydrogenation of the species with lower H content (acetylene, ethynyl). C–C bond breaking in ethynyl may be competitive with that of C_2, in line with our recent theoretical study on Pd(1 1 1) [8].

Acknowledgments

The authors thank Prof. J.A. Lercher for stimulating discussions. Zhao-Xu Chen acknowledges support by Alexander von Humboldt Foundation for a renewed stay at TU München. Hristiyan A. Aleksandrov thanks the Bulgarian National Science Fund (Contract VUH-303/07 and the National Center of Advanced Materials UNION, DO-02-82/2008). This work was supported by Deutsche Forschungs gemeinschaft and Fonds der Chemischen Industrie (Germany). We also acknowledge generous computing resources at Leibniz Rechenzentrum München.

Appendix A. Supplementary data

Supplementary data associated with this article can be found, in the online version, at doi:10.1016/j.molcata.2011.04.019.

References

[1] G.C. Bond, Metal-Catalysed Reactions of Hydrocarbons, Springer, New York, 2005.
[2] D. Stacchiola, S. Azad, L. Burkholder, W.T. Tysoe, J. Phys. Chem. B 105 (2001) 11233–11239.
[3] V. Pallassana, M. Neurock, V.S. Lusvardi, J.J. Lerou, D.D. Kragten, R.A. Van Santen, J. Phys. Chem. B 106 (2002) 1656–1669.
[4] M. Li, W. Guo, R. Jiang, L. Zhao, X. Lu, H. Zhu, D. Fu, H. Shan, J. Phys. Chem. C 114 (2010) 8440–8448.
[5] J. Andersin, N. Lopez, K. Honkala, J. Phys. Chem. C 113 (2009) 8278–8286.
[6] L.V. Moskaleva, Z.-X. Chen, H.A. Aleksandrov, A.B. Mohammed, Q. Sun, N. Rösch, J. Phys. Chem. C 113 (2009) 2512–2520.
[7] Z.-J. Zhao, L.M. Moskaleva, H.A. Aleksandrov, D. Basaran, N. Rösch, J. Phys. Chem. C 114 (2010) 12190–12201.
[8] Z.-X. Chen, H.A. Aleksandrov, D. Basaran, N. Rösch, J. Phys. Chem. C 114 (2010) 17683–17692.
[9] L.V. Moskaleva, H.A. Aleksandrov, D. Basaran, Z.-J. Zhao, N. Rösch, J. Phys. Chem. C 113 (2009) 15373–15379.
[10] V. Pallassana, M. Neurock, J. Catal. 191 (2000) 301–317.
[11] J. Andersin, K. Honkala, Surf. Sci. 604 (2010) 762–769.
[12] M. Neurock, R.A. van Santen, J. Phys. Chem. B 104 (2000) 11127–11145.
[13] R. Hirschl, A. Eichler, J. Hafner, J. Catal. 226 (2004) 273–282.
[14] Y. Chen, D.G. Vlachos, J. Phys. Chem. C 114 (2010) 4973–4982.
[15] R.T. Vang, K. Honkala, S. Dahl, E.K. Vestergaard, J. Schnadt, E. Lægsgaard, B.S. Clausen, J.K. Nørskov, F. Besenbacher, Surf. Sci. 600 (2006) 66–77.
[16] L.L. Kesmodel, L.H. Dubois, G.A. Somorjai, J. Chem. Phys. 70 (1979) 2180–2188.
[17] R.J. Koestner, M.A. Van Hove, G.A. Somorjai, Surf. Sci. 121 (1982) 321–337.
[18] L.L. Kesmodel, J.A. Gates, Surf. Sci. 111 (1981) L747–L754.
[19] T.S. Marinova, K.L. Kostov, Surf. Sci. 181 (1987) 573–585.
[20] L.P. Wang, W.T. Tysoe, R.M. Ormerod, R.M. Lambert, H. Hoffmann, F. Zaera, J. Phys. Chem. 94 (1990) 4236–4239.
[21] A.M. Goda, M.A. Barteau, J.G. Chen, J. Phys. Chem. B 110 (2006) 11823–11831.
[22] J.W. Medlin, M.D. Allendorf, J. Phys. Chem. B 107 (2003) 217–223.
[23] S. Kozlov, I.V. Yudanov, H.A. Aleksandrov, N. Rösch, Phys. Chem. Chem. Phys. 11 (2009) 10955–10963.
[24] G. Kresse, J. Hafner, Phys. Rev. B 49 (1994) 14251–14269.
[25] G. Kresse, J. Furthmüller, Comput. Mater. Sci. 6 (1996) 15–50.
[26] P.E. Blöchl, Phys. Rev. B 50 (1994) 17953–17979.
[27] G. Kresse, D. Joubert, Phys. Rev. B 59 (1999) 1758–1775.
[28] J.P. Perdew, Y. Wang, Phys. Rev. B 45 (1992) 13244–13249.
[29] H.J. Monkhorst, J.D. Pack, Phys. Rev. B 13 (1976) 5188–5192.
[30] M. Methfessel, A.T. Paxton, Phys. Rev. B 40 (1989) 3616–3621.
[31] G. Henkelman, H. Jónsson, J. Chem. Phys. 111 (1999) 7010–7022.
[32] G. Mills, H. Jónsson, G.K. Schenter, Surf. Sci. 324 (1995) 305–337.
[33] H. Jónsson, G. Mills, K.W. Jacobsen, in: B.J. Berne, G. Ciccotti, D.F. Coker (Eds.), Classical and Quantum Dynamics in Condensed Phase Simulations, World Scientific, Singapore, 1998, p. 385.
[34] S. Nave, A.K. Tiwari, B. Jackson, J. Chem. Phys. 132 (2010) 054705.
[35] In Ref. 15, a somewhat frugal model of the metal surface was used. Only the top layer of three-layer slabs was allowed to relax during structure optimization. The plane wave cutoff was set to 340 eV, and the integration in k-space used 12 k-points. The core electrons of all atoms were treated with Vanderbilt ultrasoft pseudopotentials.
[36] C.M. Mate, C.T. Kao, B.E. Bent, G.A. Somorjai, Surf. Sci. 197 (1988) 183–207.
[37] X.Y. Zhu, J.M. White, Surf. Sci. 214 (1989) 240–256.
[38] P.S. Cremer, X. Su, Y.R. Shen, G.A. Somorjai, J. Phys. Chem. B 101 (1997) 6474–6478.
[39] T.V.W. Janssens, S. Volkening, T. Zambelli, J. Wintterlin, J. Phys. Chem. B 102 (1998) 6521–6528.
[40] R.M. Ormerod, R.M. Lambert, H. Hoffmann, F. Zaera, L.P. Wang, D.W. Bennett, W.T. Tysoe, J. Phys. Chem. 98 (1994) 2134–2138.
[41] J.R. Rostrup-Nielsen, J.H.B. Hansen, J. Catal. 144 (1993) 38–49.
[42] H.S. Bengaard, J.K. Nørskov, J. Sehested, B.S. Clausen, L.P. Nielsen, A.M. Molenbroek, J.R. Rostrup-Nielsen, J. Catal. 209 (2002) 365–384.
[43] J. Xu, M. Saeys, J. Catal. 242 (2006) 217–226.
[44] J.N. Brønsted, Chem. Rev. 5 (1928) 231–338.
[45] M.G. Evans, M. Polanyi, Trans. Faraday Soc. 34 (1938) 0011–0023.
[46] Z.-P. Liu, P. Hu, J. Chem. Phys. 114 (2001) 8244–8247.
[47] J.K. Nørskov, T. Bligaard, A. Logadottir, S. Bahn, L.B. Hansen, M. Bollinger, H. Bengaard, B. Hammer, Z. Sljivancanin, M. Mavrikakis, Y. Xu, S. Dahl, C.J.H. Jacobsen, J. Catal. 209 (2002) 275–278.
[48] A. Michaelides, Z.P. Liu, C.J. Zhang, A. Alavi, D.A. King, P. Hu, J. Am. Chem. Soc. 125 (2003) 3704–3705.
[49] H.-F. Wang, Z.-P. Liu, J. Am. Chem. Soc. 130 (2008) 10996–11004.
[50] G.S. Hammond, J. Am. Chem. Soc. 77 (1955) 334–338.
[51] D.H. Mei, P.A. Sheth, M. Neurock, C.M. Smith, J. Catal. 242 (2006) 1–15.
[52] S.G. Podkolzin, R. Alcala, J.J. de Pablo, J.A. Dumesic, J. Phys. Chem. B 106 (2002) 9604–9612.
[53] G.A. Somorjai, Introduction to Surface Chemistry and Catalysis, First ed., Wiley, 1994.
[54] J. Xu, M. Saeys, J. Phys. Chem. C 113 (2009) 4099–4106.